

Resolving Continua of Fractional Excitations by Spinon Echo in THz 2D Coherent Spectroscopy

Yuan Wan^{1,*} and N. P. Armitage^{2,3,†}

¹Institute of Physics, Chinese Academy of Sciences, Beijing 100190, China

²Institute for Quantum Matter and Department of Physics and Astronomy, Johns Hopkins University, Baltimore, Maryland 21218, USA

³Institute for Solid State Physics, University of Tokyo, Kashiwa 277-8581, Japan



(Received 3 December 2018; published 25 June 2019)

We show that the new technique of terahertz 2D coherent spectroscopy is capable of giving qualitatively new information about fractionalized spin systems. For the prototypical example of the transverse field Ising chain, we demonstrate theoretically that, despite the broad continuum of excitations in linear response, the 2D spectrum contains sharp features that are a coherent signature of a “spinon echo,” which gives previously inaccessible information such as the lifetime of the two-spinon excited state. The effects of disorder and finite lifetime, which are practically indistinguishable in the linear optical or neutron response, manifest in dramatically different fashion in the 2D spectra. Our results may be directly applicable to model quasi-1D transverse field Ising chain systems such as CoNb_2O_6 , but the concept can be applied to fractionalized spin systems in general.

DOI: 10.1103/PhysRevLett.122.257401

In recent years, wholly new classes of condensed matter systems have become of intense interest. Topological materials, quantum spin liquids, and strange metals are characterized by Berry phase effects, fractional excitations, and highly entangled ground states [1–4]. However, we can measure many of their correlations only imperfectly with existing tools. A promising direction is nonlinear response that has been used to characterize the symmetry of semiconductors [5] and magnets [6], Berry phase in topological semimetals [7–9], and exotic ground states and excitations in correlated systems [10–12].

For quantum spin liquids, one of their most remarkable properties is the emergence of fractional particles known as spinons that may be understood as carrying half a conventional spin degree of freedom. Spinons present a challenge for conventional spectroscopy as they must be excited in pairs. This typically leads to a broad continuum spectrum that represents a convolution of all possible ways that energy and momentum can be shared between two spinons. In conventional linear magnetic susceptibility $\chi^{(1)}(\omega)$ of a spin chain [13], light excites a pair of spinons with opposite momenta [Fig. 1(a)]. Each pair gives rise to a peak in the absorption spectrum $\text{Im}\chi^{(1)}$ centered at the frequency $\omega = \lambda_{\mathbf{k}} + \lambda_{-\mathbf{k}}$, where $\lambda_{\mathbf{k}}$ is the dispersion relation of the spinon. As there are infinitely many such pairs, the absorption peaks congest the frequency axis, resulting in a broad continuum [Fig. 1(b), top]. While the broad continuum seen with terahertz (THz) optical spectroscopy and neutron scattering has reasonably been taken as evidence for spinons in spin chains [13–15], the situation is less straightforward in higher-dimensional spin liquid candidates, e.g., 2D Kitaev materials, Herbertsmithite, and

triangular lattices [16–21]. In such cases, the relative importance of finite lifetime and disorder and even fractionalization itself is unclear. In all cases, the intrinsic spectral properties of spinons such as the linewidth and shape are hidden in the continuum.

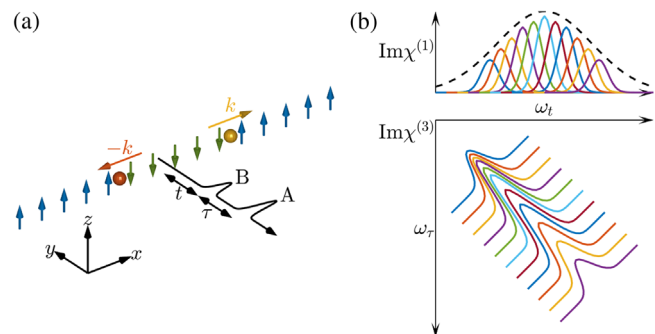


FIG. 1. (a) The experimental setup for THz 2D coherent spectroscopy. Two linearly polarized magnetic field pulses A and B arrive at the sample [in this case, TFIC] at time 0 and τ . Magnetization is recorded at time $\tau + t$. In the FM phase, the pulses excite a pair of spinons (domain walls) with momenta $\pm\mathbf{k}$. (b) Top: 1D spectroscopy probes the linear magnetic susceptibility $\chi^{(1)}(\omega)$ of TFIC. Each pair of spinons with momenta $\pm\mathbf{k}$ gives an absorption peak. The peaks congest the frequency axis, resulting in a spinon continuum. Bottom: 2D spectroscopy probes nonlinear magnetic susceptibilities of the TFIC. The signal due to the third order susceptibility $\chi^{(3)}(\omega_t, \omega_\tau)$ can resolve the spinon continuum by spreading it into the frequency plane. Spectral congestion occurs along the diagonal, whereas the width of the individual resonance peak is revealed along the antidiagonal direction.

In this work, we show that the new technique of THz two-dimensional coherent spectroscopy (2DCS) [22,23] can provide qualitatively new information on the dynamical properties of spinons. We explore our ideas in the context of the simplest minimal model for fractionalization—the transverse field Ising chain (TFIC)—but the possibilities are more general. In the optical and radio frequency range [24–27], 2DCS is an established technique that probes nonlinear susceptibilities. Thanks to recent technical advances that enable tabletop high-intensity THz sources, it has been extended recently to the THz range to study graphene and quantum wells [22,23], molecular rotations [28], and spin waves in the conventional magnet YFeO₃ [29]. THz 2DCS uses two pulses in a collinear geometry to excite a system at one frequency and detect at another, thus producing a 2D spectrum. Applications of 2DCS include quantifying nonlinear couplings between excitations and—relevant to the present work—separating inhomogeneous and homogeneous broadening [25–27]. A similar mechanism will allow for the resolution of the spinon continuum in the 2D spectrum [Fig. 1(b), bottom], where congestion occurs along the 2D spectrum’s diagonal, but the intrinsic linewidth of each spinon pair is revealed by the spectral width along the antidiagonal.

The TFIC Hamiltonian is [30]

$$H = -J \left(\sum_{n=1}^{L-1} \sigma_n^z \sigma_{n+1}^z + \eta \sigma_L^z \sigma_1^z \right) - h \sum_n \sigma_n. \quad (1)$$

Here, $\sigma_n^{x,y,z}$ are Pauli matrices, $J > 0$ is the ferromagnetic exchange, $h > 0$ is the transverse field, and L is the chain length. We shall use periodic ($\eta = 1$) and open ($\eta = 0$) boundary conditions as they suit our purposes. Macroscopic response functions are independent of such choices. This system admits a twofold degenerate ferromagnetic (FM) ground state for $h < J$ and a single paramagnetic (PM) ground state for $h > J$. While strictly speaking, the TFIC is not a spin liquid—the domain wall excitations of the FM phase are close analogues of spinons. Henceforth, we use “domain wall” and “spinon” interchangeably.

We consider a setup similar to that used in Ref. [29]. Two linearly polarized magnetic field pulses A and B arrive at the sample at time 0 and $\tau > 0$ [Fig. 1(a)]. The magnetization at time $\tau + t$ along direction α , $M_{AB}^\alpha(\tau + t)$, is a convolution of applied field with the sample response [31]. The experiment is then repeated but with pulse A or B alone and the magnetization recorded as $M_A^\alpha(\tau + t)$ and $M_B^\alpha(\tau + t)$. The nonlinear signal is defined as $M_{NL}^\alpha(t, \tau) = M_{AB}^\alpha(\tau + t) - M_A^\alpha(\tau + t) - M_B^\alpha(\tau + t)$. The 2D spectrum is the Fourier transform (FT) of $M_{NL}^\alpha(t, \tau)$ over the domain $t > 0, \tau > 0$.

The nonlinear magnetization $M_{NL}^\alpha(t, \tau)$ is a direct measure of the second and/or third order magnetic susceptibilities. For simplicity, we model the magnetic field as two Dirac- δ pulses with the same polarization β , i.e., $B^\beta(s) = A_0^\beta \delta(s) + A_\tau^\beta \delta(s - \tau)$, where s is time and $A_{0,\tau}^\beta$ the pulse

areas. In principle, the polarizations of pulses A and B can be different. The nonlinear signal (see Supplemental Material [32]) is

$$\begin{aligned} M_{NL}^\alpha(t, \tau) = & A_0^\beta A_\tau^\beta \chi_{\alpha\beta\beta}^{(2)}(t, \tau + t) \\ & + (A_0^\beta)^2 A_\tau^\beta \chi_{\alpha\beta\beta\beta}^{(3)}(t, \tau + t, \tau + t) \\ & + A_0^\beta (A_\tau^\beta)^2 \chi_{\alpha\beta\beta\beta}^{(3)}(t, t, \tau + t) + O(A^4). \end{aligned} \quad (2)$$

Here, we have retained the dominant and subdominant contributions. The two $\chi^{(3)}$ terms encode different physical processes. In the first, pulse A couples to the sample at second order, whereas pulse B couples at first order. In the second, the contributions of A and B are switched.

We are primarily interested in the spinons in the FM phase at zero temperature, and thus, we use the representative model parameters $h/(h + J) = 0.3$ in the ensuing discussion. Since σ_n^x excites spinon pairs, we focus on the polarization $\alpha = \beta = \hat{x}$. We calculate $\chi_{xxx}^{(2)}$ and $\chi_{xxxx}^{(3)}$ analytically through the following procedure (see the Supplemental Material [32] for details). We map Eq. (1) to free fermionic spinons by using the Jordan-Wigner transformation [30]. Each pair of spinons with momenta $\pm k$ form a two-level system (TLS), whose ground (excited) state corresponds to the absence (presence) of the said pair. The energy level splitting is $2\lambda_k$, where $\lambda_k = 2\sqrt{J^2 + h^2 + 2Jh \cos k}$ is the spinon dispersion. As the TLSs formed by different spinon pairs are decoupled, the TFIC is equivalent to an ensemble of independent TLSs, thereby permitting a straightforward calculation of the nonlinear response [27].

In more realistic models, additions to Eq. (1) such as additional exchange interactions and spin-lattice couplings induce spinon interactions, which give effects such as spinon decay. By the TLS analogy, we incorporate these effects phenomenologically through a population time T_1 and decoherence time T_2 [5], which captures the essential physics while maintaining the analytic tractability [32]. We assume $T_{1,2}$ are k independent for simplicity. The ideal TFIC then corresponds to $T_{1,2} = 0$.

We begin with the linear susceptibility per site,

$$\chi_{xx}^{(1)}(t) = \frac{2\theta(t)}{L} \sum_{k>0} \sin^2 \theta_k e^{-t/T_2} \sin(2\lambda_k t), \quad (3)$$

where $\sin \theta_k = -2J \sin k / \lambda_k$ is the optical matrix element. The summation is over the positive half of the first Brillouin zone (1BZ). Using the above TLS picture, we interpret Eq. (3) as follows. The magnetic field pulse induces optical transitions in all TLSs, producing a damped oscillatory signal with frequency $2\lambda_k$. The damping coefficient $1/T_2$ reflects the spinon decay. Since the frequency takes its value from a dense spectrum given by k , dephasing leads to

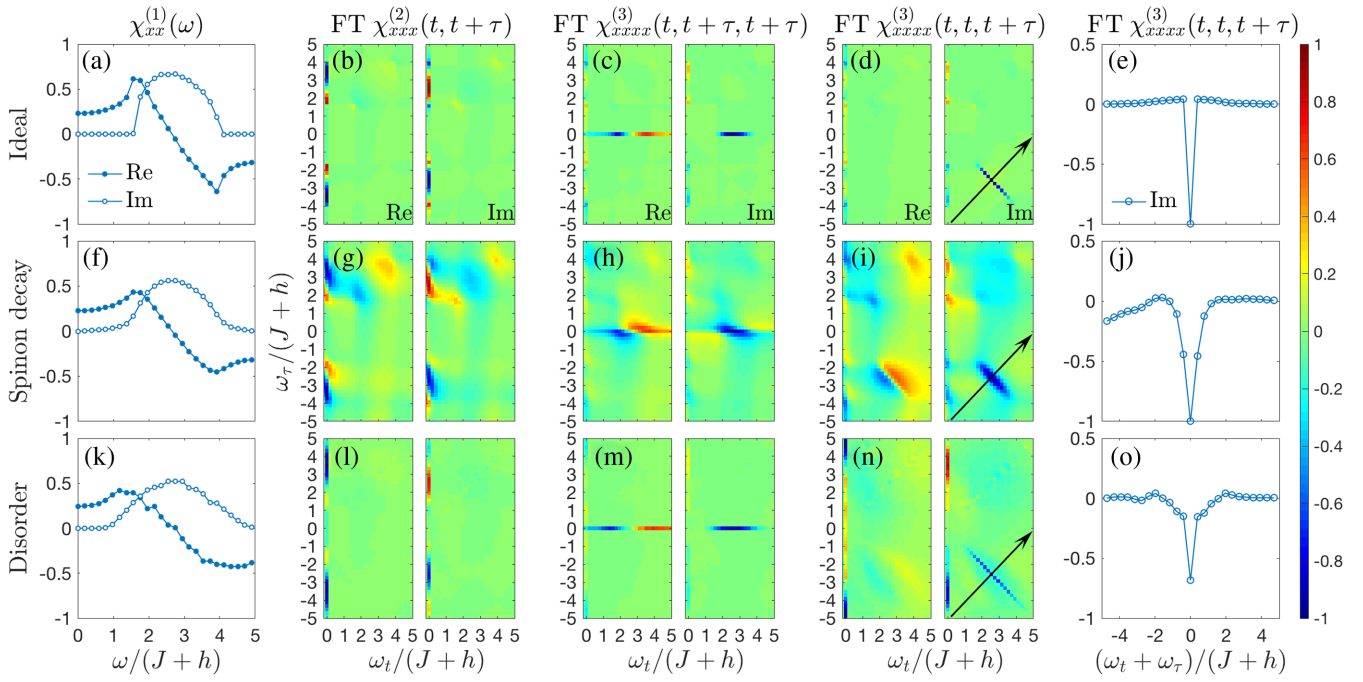


FIG. 2. 1D and 2D spectra in the FM phase [$h/(h+J) = 0.3$] of the TFIC. From the top to bottom, the rows show (a–e) the case with no dissipation ($1/T_{1,2} = 0$), (f–j) with dissipation [$1/T_{1,2} = 0.2(J+h)$ (other values of $T_{1,2}$ bring no significant changes)], and (k–o) with quenched disorder. From the left to right, the columns show, respectively, $\chi_{xx}^{(1)}(\omega)$, and the FTs of $\chi_{xxx}^{(2)}(t, t+\tau)$, $\chi_{xxxx}^{(3)}(t, \tau+t, \tau+t)$, $\chi_{xxxx}^{(3)}(t, t, \tau+t)$, and its profile along a cut indicated by the arrow. Only half of the frequency plane is shown; the other half is related by complex conjugation. For the cases without disorder (top, middle rows), the calculation is done on a chain of $L = 100$ with the periodic boundary condition. For the disorder case (bottom row), we set $h_n = ha_n$ and $J_n = Jb_n$, where a_n, b_n are site-dependent dimensionless random numbers drawn uniformly from the interval (0.5, 1.5). The spectra are calculated for a chain of $L = 40$ with open boundaries and averaged over 200 disorder realizations.

an additional decay of $\chi_{xx}^{(1)}(t)$, which is difficult to distinguish from the intrinsic decay due to finite T_2 . This difficulty of unraveling the dephasing and the intrinsic decay persists in the frequency domain. Here, each spinon pair contributes an absorption peak in $\text{Im}\chi_{xx}^{(1)}$ centered at the energy $2\lambda_k$ with width $1/T_2$. As k runs over the 1BZ, the peaks form a broad continuum, which disguises the intrinsic linewidth $1/T_2$. Comparing the continuum for $1/T_2 = 0$ [Fig. 2(a)] and $1/T_2 = 0.2(J+h)$ [Fig. 2(f)], the difference is merely quantitative.

We then turn to the lowest order nonlinear response:

$$\begin{aligned} \chi_{xxx}^{(2)}(t, \tau+t) &= \frac{4\theta(t)\theta(\tau)}{L} \sum_{k>0} \sin^2 \theta_k \cos \theta_k \\ &\times \{ e^{-t/T_1} \cos(2\lambda_k \tau) \\ &- e^{-(t+\tau)/T_2} \cos[2\lambda_k(\tau+t)] \}. \end{aligned} \quad (4)$$

The first term on the right-hand side of Eq. (4) is non-oscillatory in t . In the frequency domain, this gives rise to a peak centered at $\omega_t = 0$, appearing as the streak along the ω_τ axis shown in Fig. 2(b). Increasing $1/T_1$ from 0 leads to broadening of the streak [Fig. 2(g)]. Viewing ω_τ as the

pumping frequency and ω_t the detecting frequency, this streak is a THz rectification (TR) signal [29]. The second term of Eq. (4) is oscillatory in $t + \tau$. Yet, similar to Eq. (3), the dephasing leads to decay, which is further modulated by the intrinsic decay due to T_2 . This results in a diffusive, barely discernible signal in the first frequency quadrant [Figs. 2(b) and 2(g)], which is similar to the nonrephasing (NR) signal usually found in $\chi^{(3)}$ [29]. See the Supplemental Material [32] for a detailed discussion of these features.

Qualitatively different physics appears in $\chi_{xxxx}^{(3)}$. It is instructive to consider the more general form that corresponds to a three-pulse process [Fig. 3(a)]: $\chi_{xxxx}^{(3)}(t_3, t_2+t_3, t_1+t_2+t_3) = -[\theta(t_1)\theta(t_2)\theta(t_3)/L] \sum_{k>0} A_k^{(1)} + A_k^{(2)} + A_k^{(3)} + A_k^{(4)}$, where

$$\begin{aligned} A_k^{(1)} &= 8 \sin^2 \theta_k \cos^2 \theta_k \sin[2\lambda_k(t_3+t_2+t_1)] \\ &\times e^{-(t_1+t_2+t_3)/T_2}, \end{aligned} \quad (5a)$$

$$\begin{aligned} A_k^{(2)} &= -8 \sin^2 \theta_k \cos^2 \theta_k \sin[2\lambda_k(t_2+t_1)] \\ &\times e^{-(t_1+t_2)/T_2} e^{-t_3/T_1}, \end{aligned} \quad (5b)$$

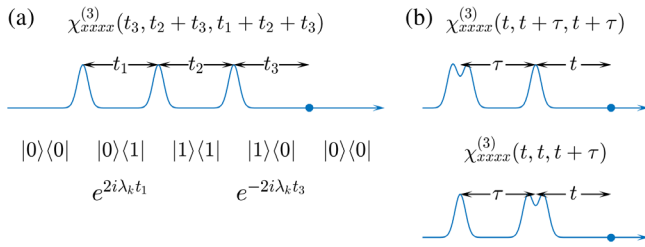


FIG. 3. (a) Three-pulse process associated with $\chi_{xxxx}^{(3)}(t_3, t_2 + t_3, t_1 + t_2 + t_3)$. The spinon echo process that produces the rephasing signal $A_k^{(4)}$ [Eq. (5)] is also shown. 0 (1) stands for the ground (excited) state of the two-level system formed by the spinon pair $\pm k$. The density matrices during t_1 and t_3 are Hermitian conjugate partners, and thus, their time evolutions are effectively time reversals of each other. (b) The $\chi^{(3)}$ terms measured in the two-pulse setup [Eq. (2)] are special limits of the three-pulse process.

$$A_k^{(3)} = 4 \sin^4 \theta_k \sin[2\lambda_k(t_3 + t_1)] \times e^{-(t_1+t_3)/T_2} e^{-t_2/T_1}, \quad (5c)$$

$$A_k^{(4)} = 4 \sin^4 \theta_k \sin[2\lambda_k(t_3 - t_1)] \times e^{-(t_1+t_3)/T_2} e^{-t_2/T_1}. \quad (5d)$$

$A_k^{(1-4)}$ encode distinct evolution paths of the density matrix of the spinon pair with momenta $\pm k$ due to the THz pulses. While the forms of $A_k^{(1,2,3)}$ resemble that of $\chi_{xxx}^{(2)}$, $A_k^{(4)}$ is different in that t_1 and t_3 appear with opposite signs. Regardless of the oscillation frequency $2\lambda_k$, the phase accumulated between the first and the second pulses (t_1) is canceled after the third pulse at $t_3 = t_1$. Said differently, the dephasing process during t_1 is countered by the rephasing process during t_3 . This rephasing process is the incarnation of the photon echo in the context of spinon dynamics. Tracing $A_k^{(4)}$ back to its originating density matrix evolution sequence [Fig. 3(a)], we find the sequence is identical to the photon echo process from a TLS [27,39]. Therefore, we term this process the “spinon echo.”

Photon echo and its analogues are a sensitive diagnostics of dissipation [27,39]. Here, the rephasing signal from the spinon echo allows for a direct measurement of T_2 . To see this, we return to the $\chi_{xxxx}^{(3)}$ measured in the two-pulse setup [Eq. (2)]. $\chi_{xxxx}^{(3)}(t, t, \tau + t)$ corresponds to the limit $t_1 \rightarrow \tau$, $t_2 \rightarrow 0$, $t_3 \rightarrow t$ [Fig. 3(b)]. We may write $\sum_k A_k^{(4)} = f(t - \tau) \exp[-(t + \tau)/T_2]$, where $f(t - \tau)$ comes from the sum of $\sin^4 \theta_k \sin[2\lambda_k(t - \tau)]$ and decreases as $|t - \tau|$ increases due to dephasing. Crucially, the arguments of f and the T_2 term are *orthogonal* linear combinations of t and τ . The FT of f is a broad continuum that depends on $\omega_t - \omega_\tau$, whereas the FT of the T_2 term is a narrow Lorentzian function of $\omega_t + \omega_\tau$. The product of the two

thus gives rise to a streak of rephasing signal in the imaginary part of the FT of $\chi_{xxxx}^{(3)}(t, \tau + t)$. The streak runs along the diagonal of the fourth quadrant, mirroring the energy range of spinon pairs. The width of the streak along the antidiagonal is a direct measure of $1/T_2$: In the limit of $T_2 \rightarrow 0$, the antidiagonal width vanishes, reflecting the perfect phase cancellation in the spinon echo [Figs. 2(d) and 2(e)]. With finite T_2 , imperfect phase cancellation leads to a finite antidiagonal width that scales with $1/T_2$ [Figs. 2(f) and 2(g)].

By contrast, $\chi_{xxxx}^{(3)}(t, \tau + t, \tau + t)$ corresponding to the limit $t_1 \rightarrow 0$, $t_2 \rightarrow \tau$, $t_3 \rightarrow t$ does not contain a spinon echo [Fig. 3(b)]. In the limit of $1/T_1 \rightarrow 0$, $A_k^{(3,4)}$ are functions of $t_3 = t$ only. In the frequency domain, this leads to a Dirac- δ peak on the $\omega_\tau = 0$ line, which appears in the imaginary part as a streak along the ω_t axis [Fig. 2(c)]. Taking $\omega_\tau(\omega_t)$ as the pumping (detecting) frequency, this may be interpreted as a pump-probe signal [29]. Increasing $1/T_1$ broadens the signal [Fig. 2(h)].

Both $\chi_{xxxx}^{(3)}$ s contain additional features that arise from $A_k^{(1,2,3)}$ terms in Eq. (5). Their FTs contain a diffusive, weak NR signal in the first quadrant. They also contain a weak TR-like signal on the ω_τ axis, which we discuss further in the Supplemental Material [32].

To recap, the rephasing signal from the spinon echo process can directly reveal the T_2 time of spinon pairs. Crucially, in the absence of dissipation ($1/T_{1,2} = 0$), the antidiagonal width of the rephasing signal is zero. We now show that this feature is robust against quenched disorder. To this end, we set the transverse field h_n and exchange constant J_n to be site dependent, namely, $h_n = ha_n$, $J_n = Jb_n$, where a_n, b_n are dimensionless random numbers drawn from a uniform distribution in the interval [0.5, 1.5]. The linear response [Fig. 2(k)] shows only small changes compared to the clean case. Since this model remains integrable, the spinons are still exact eigenstates, and therefore, the antidiagonal width of the rephasing signal remains resolution limited [Figs. 2(n) and 2(o)]. Its strong sensitivity to dissipation protected by the robustness against disorder shows the utility of 2DCS.

In the FM phase, the σ_n^y operators can also excite spinon pairs. We therefore expect the 2DCS spectrum with \hat{y} polarization to be similar to \hat{x} . However, since the σ_n^y is a nonlocal operator in the spinon basis, the analytic treatment made for \hat{x} does not translate directly to \hat{y} . Nevertheless, as shown in the Supplemental Material [32], the numerical calculation finds that the 2D spectra along \hat{y} in the FM phase (Supplemental Material Fig. S4 [32]) are qualitatively similar to that of \hat{x} . Note that in the PM phase, the streaklike rephasing signal that is characteristic of fractional excitations is absent. $\chi_{yyy}^{(3)}$ instead shows sharp isolated peaks [32] that are typical of nonlinear spin waves [12,29].

Using the TFIC as a prototypical example, we have demonstrated that THz 2DCS can resolve the spinon

continuum and directly reveal the intrinsic linewidth of spinon pairs. We expect spinon echo to be a generic 2D spectral feature of models that host spinons. Provided that the spinons are coherent quasiparticles, the TLS picture naturally extends to higher-dimensional spin liquids. In general, spinon echo will produce a rephasing streak qualitatively similar to that of the TFIC with finite $T_{1,2}$. In particular, the finite antidiagonal width of the streak reflects the imperfect phase cancellation due to finite quasiparticle lifetime.

Our results may be applicable to CoNb_2O_6 , which is the best-known material example of a quasi-1D FM Ising chain [13,15,40]. CoNb_2O_6 orders at temperatures below ~ 3 K, but at slightly higher temperatures, the linear response is characterized by a broad line shape made of superimposed two- and four-spinon continua that hide information about spinon line shapes. We expect that THz 2DCS can reveal the intrinsic spectral properties of spinons in this system. Experiments can be done in essentially the same fashion as previous THz 2DCS measurements on the conventional magnet YFeO_3 [29]. Such experiments are under way. Analyzing theoretically the 2D spectra of more realistic material models will also prove fruitful. The spinon interactions present in these models will produce additional spectral features that are beyond the minimal model considered here.

With the information gained by establishing the technique on TFIC and its material realizations, we expect even richer information can be gained by applying THz 2DCS to higher-dimensional materials that are suspected to harbor a spin liquid but have only been characterized spectroscopically as having broad line shapes such as Herbertsmithite [16], 2D Kitaev magnets [17], and triangular lattices [18–21]. By direct analogy to the present results, we expect that one can measure the intrinsic lifetime of the multispinon excitations. Sharp antidiagonal features may give direct evidence for fractionalized excitations and may be readily distinguished from highly damped conventional spin waves that could alternatively be present. Finally, we want to stress that our work is just an early step in understanding the utility of THz 2DCS for quantum materials. We believe important applications will be found in many systems including superconductors and topological materials.

We thank F. Mahmood, P. Orth, M. Oshikawa, and Y. Sizuk for discussions. Y. W. thanks for the support of the National Supercomputer Center in Tianjin, China. The numerical calculations were performed on TianHe-1A. N. P. A. was supported as part of the Institute for Quantum Matter, an Energy Frontier Research Center funded by the U.S. Department of Energy, Office of Basic Energy Science under Grant No. DE-SC0019331. N. P. A. acknowledges additional support from the Japan Society for the Promotion of Science, International Research Fellows Program.

^{*}yuan.wan@iphy.ac.cn

[†]npa@jhu.edu

- [1] L. Balents, *Nature (London)* **464**, 199 (2010).
- [2] D. Xiao, M.-C. Chang, and Q. Niu, *Rev. Mod. Phys.* **82**, 1959 (2010).
- [3] L. Savary and L. Balents, *Rep. Prog. Phys.* **80**, 016502 (2017).
- [4] N. P. Armitage, E. J. Mele, and A. Vishwanath, *Rev. Mod. Phys.* **90**, 015001 (2018).
- [5] Y. R. Shen, *The Principles of Nonlinear Optics*, 1st ed. (Wiley-Interscience, New York, 1984).
- [6] M. Fiebig, V. V. Pavlov, and R. V. Pisarev, *J. Opt. Soc. Am. B* **22**, 96 (2005).
- [7] J. E. Sipe and A. I. Shkrebtii, *Phys. Rev. B* **61**, 5337 (2000).
- [8] T. Morimoto and N. Nagaosa, *Sci. Adv.* **2**, e1501524 (2016).
- [9] J. E. Moore and J. Orenstein, *Phys. Rev. Lett.* **105**, 026805 (2010).
- [10] L. Zhao, C. A. Belvin, R. Liang, D. A. Bonn, W. N. Hardy, N. P. Armitage, and D. Hsieh, *Nat. Phys.* **13**, 250 (2017).
- [11] L. Zhao, D. H. Torchinsky, H. Chu, V. Ivanov, R. Lifshitz, R. Flint, T. Qi, G. Cao, and D. Hsieh, *Nat. Phys.* **12**, 32 (2016).
- [12] H. M. Babujian, M. Karowski, and A. M. Tsvelik, *Phys. Rev. B* **94**, 155156 (2016).
- [13] C. M. Morris, R. Valdés Aguilar, A. Ghosh, S. M. Koohpayeh, J. Krizan, R. J. Cava, O. Tchernyshyov, T. M. McQueen, and N. P. Armitage, *Phys. Rev. Lett.* **112**, 137403 (2014).
- [14] B. Lake, D. A. Tennant, C. D. Frost, and S. E. Nagler, *Nat. Mater.* **4**, 329 (2005).
- [15] R. Coldea, D. A. Tennant, E. M. Wheeler, E. Wawrzynska, D. Prabhakaran, M. Telling, K. Habicht, P. Smeibidl, and K. Kiefer, *Science* **327**, 177 (2010).
- [16] T.-H. Han, J. S. Helton, S. Chu, D. G. Nocera, J. A. Rodriguez-Rivera, C. Broholm, and Y. S. Lee, *Nature (London)* **492**, 406 (2012).
- [17] A. Banerjee, J. Yan, J. Knolle, C. A. Bridges, M. B. Stone, M. D. Lumsden, D. G. Mandrus, D. A. Tennant, R. Moessner, and S. E. Nagler, *Science* **356**, 1055 (2017).
- [18] Y. Shen, Y.-D. Li, H. Wo, Y. Li, S. Shen, B. Pan, Q. Wang, H. C. Walker, P. Steffens, M. Boehm, Y. Hao, D. L. Quintero-Castro, L. W. Harriger, M. D. Frontzek, L. Hao, S. Meng, Q. Zhang, G. Chen, and J. Zhao, *Nature (London)* **540**, 559 (2016).
- [19] J. A. M. Paddison, M. Daum, Z. Dun, G. Ehlers, Y. Liu, M. B. Stone, H. Zhou, and M. Mourigal, *Nat. Phys.* **13**, 117 (2017).
- [20] X. Zhang, F. Mahmood, M. Daum, Z. Dun, J. A. M. Paddison, N. J. Laurita, T. Hong, H. Zhou, N. P. Armitage, and M. Mourigal, *Phys. Rev. X* **8**, 031001 (2018).
- [21] Z. Zhu, P. A. Maksimov, S. R. White, and A. L. Chernyshev, *Phys. Rev. Lett.* **119**, 157201 (2017).
- [22] W. Kuehn, K. Reimann, M. Woerner, T. Elsaesser, and R. Hey, *J. Phys. Chem. B* **115**, 5448 (2011).
- [23] M. Woerner, W. Kuehn, P. Bowlan, K. Reimann, and T. Elsaesser, *New J. Phys.* **15**, 025039 (2013).
- [24] W. Aue, E. Bartholdi, and R. R. Ernst, *J. Chem. Phys.* **64**, 2229 (1976).
- [25] S. T. Cundiff and S. Mukamel, *Phys. Today* **66**, No. 7, 44 (2013).

- [26] P. Hamm and M. Zanni, *Concepts and Methods of 2D Infrared Spectroscopy* (Cambridge University Press, Cambridge, England, 2011).
- [27] S. Mukamel, *Principles of Nonlinear Optical Spectroscopy*, Oxford Series in Optical and Imaging Sciences (Oxford University Press, New York, 1999), Vol. 6.
- [28] J. Lu, Y. Zhang, H. Y. Hwang, B. K. Ofori-Okai, S. Fleischer, and K. A. Nelson, *Proc. Natl. Acad. Sci. U.S.A.* **113**, 11800 (2016).
- [29] J. Lu, X. Li, H. Y. Hwang, B. K. Ofori-Okai, T. Kurihara, T. Suemoto, and K. A. Nelson, *Phys. Rev. Lett.* **118**, 207204 (2017).
- [30] P. Pfeuty, *Ann. Phys. (N.Y.)* **57**, 79 (1970).
- [31] Note that we use definitions of t and τ consistent with that of Ref. [29] but different from that of Refs. [22].
- [32] See Supplemental Material at <http://link.aps.org/supplemental/10.1103/PhysRevLett.122.257401> for details of the calculation procedure, which also includes Refs. [5,27,29,30,33–38].
- [33] B. M. McCoy, E. Barouch, and D. B. Abraham, *Phys. Rev. A* **4**, 2331 (1971).
- [34] O. Derzhko and T. Krokhmalskii, *Phys. Rev. B* **56**, 11659 (1997).
- [35] A. Y. Kitaev, *Phys. Usp.* **44**, 131 (2001).
- [36] M. Wimmer, *ACM. Trans. Math. Softw.* **38**, 30 (2012).
- [37] A. Tomakoff, Nonlinear spectroscopy, <http://tdqms.uchicago.edu/page/nonlinear-and-two-dimensional-spectroscopy-notes>.
- [38] W. Kühn, Ph.D. thesis, Humboldt-Universität zu Berlin, 2011.
- [39] N. A. Kurnit, I. D. Abella, and S. R. Hartmann, *Phys. Rev. Lett.* **13**, 567 (1964).
- [40] J. Viirok, D. Hüvonen, T. Room, U. Nagel, C. Morris, S. Koohpayeh, T. McQueen, J. Krizan, R. Cava, and N. Armitage (to be published).